International Journal of Fluid Machinery and Systems
Vol. 8, No. 4, October-December 2015

DOI: 10.5293/IJFMS.2015.8.4.283
ISSN (Online): 1882-9554

Original Paper

Quantitative and qualitative analysis of the flow field development through T99 draft tube caused by optimized inlet velocity profiles.

Sergio Galván[1], Marcelo Reggio[2], François Guibault[3] and Gildardo Solorio[1]

[1]Mechanical Eng. Dep. Universidad Michoacana de Sán Nicolás de Hidalgo, Apdo. Postal 588 Col Centro, Morelia Mich. Mex., C.P.58001, srgalvan@umich.mx, gdiaz@umich.mx
[2]Mechanical Eng. Dep. École Polytechnique de Montréal, P.O. Box 6000, Succursale Centre Ville Montréal, QC, Canada, H3C, marcelo.reggio@polymtl.ca
[3]Computer and Software Eng. Dep. École Polytechnique de Montréal, P.O. Box 6000, Succursale Centre Ville Montréal, QC, Canada, H3C 3A7, francois.guibault@polymtl.ca

Abstract

The effect of the inlet swirling flow in a hydraulic turbine draft tube is a very complex phenomenon, which has been extensively investigated both theoretically and experimentally. In fact, the finding of the optimal flow distribution at the draft tube inlet in order to get the best performance has remained a challenge. Thus, attempting to answer this question, it was assumed that through an automatic optimization process a Genetic Algorithm would be able to manage a parameterized inlet velocity profile in order to achieve the best flow field for a particular draft tube. As a result of the optimization process, it was possible to obtain different draft-tube flow structures generated by the automatic manipulation of parameterized inlet velocity profiles. Thus, this work develops a qualitative and quantitative analysis of these new draft tube flow field structures provoked by the redesigned inlet velocity profiles. The comparisons among the different flow fields obtained clearly illustrate the importance of the flow uniformity at the end of the conduit. Another important aspect has been the elimination of the re-circulating flow area which used to promote an adverse pressure gradient in the cone, deteriorating the pressure recovery effect. Thanks to the evolutionary optimization strategy, it has been possible to demonstrate that the optimized inlet velocity profile can suppress or mitigate, at least numerically, the undesirable draft tube flow characteristics. Finally, since there is only a single swirl number for which the objective function has been minimized, the energy loss factor might be slightly affected by the flow rate if the same relation of the axial-tangential velocity components is maintained, which makes it possible to scale the inlet velocity field to different operating points.

Keywords: Numerical optimization, Draft Tubes, Hydraulic Turbines, Genetic Algorithm.

1. Introduction

In hydropower plants, the runner which drives the generator, is undoubtedly a key element of the energy conversion process, because the amount of power produced by a turbine is basically equal to the change in angular momentum across this component. Namely, the power generated by a hydraulic turbine will not only depend on the runner energy conversion, but also on the flow field quality ingested by the draft tube. Theoretically, the flow exiting the runner should have zero swirl [1]; however, this is not achievable in practice and, the power converted by the runner could be distorted by the flow delivered to the draft tube.

In this additional device, the flow leaving the runner loses its velocity, transforming the excess of kinetic energy into static pressure. This energy conversion has a significant impact on the overall turbine efficiency and power, especially for low head (high specific velocity) machines [2] and for machines operating away from their best efficiency point.

However, the effect of the inlet flow on the flow pattern in a hydraulic turbine draft tube is a very complex phenomenon, which has been extensively investigated both theoretically and experimentally. These investigations have been mainly focused on the effects of the inlet swirling flow on the inception of draft tube surging phenomenon [3-8] and in more recent years, on the draft tube performance [9-12].

Received August 24 2015; revised August 24 2015; accepted for publication November 30 2015: Review conducted by Prof. Yoshinobu Tsujimoto. (Paper number O15069S)
Corresponding author: Sergio Galván, srgalvan@umich.mx

This paper was presented at the 27th IAHR Symposium on Hydraulic Machinery and Systems, September 4, Montreal, Canada.

Among them, [10] presented an important study related to the inlet flow profile optimization. This researcher observed that to improve the pressure recovery factor required an inlet solid body swirl with moderate intensity. He tried to find the optimal inlet swirl profile for the draft tube geometry. The parameters to define the solid body swirl profile at the inlet were: the solid body swirl ratio, the radial component ratio and the axial profile uniformity. It was assumed that the three components vary linearly in the radial direction. This investigator found the efficiency to be highly sensitive to all three parameters. This study concluded that the inlet flow profile needed to be optimized to achieve the best static pressure recovery factor when the existing draft tube cannot be modified.

Recent investigations have revealed the swirling flow structure downstream a runner, by analyzing experimental data. Axial and tangential velocity profiles downstream a runner have been matched with analytic profiles given by the same set of equations. More specifically [13] proposed an outlet runner swirl criteria to avoid an unexpected sudden efficiency drop at certain discharge. This study included the axial and circumferential velocity components at the runner outlet for 17 operating points. It was shown that the swirling flow at the runner outlet for a Francis turbine can reasonably be represented using a superposition of elementary vortices.

Even though the numerical approaches of those authors concerns a Francis draft tube, there is evidence to show that the set of equations given in Ref. [13] can be applied to an axial turbine to investigate and improve draft tube performance. [14] and [15], matched the experimental axial and tangential velocity profiles downstream of a Kaplan runner with the analytical profiles. The authors found that the experimental and analytical curve shapes match, but that additional vortex functions should be included to represent the blade-tip vortex in the axial velocity profile. [16] computed the swirling flow at the T99 Kaplan runner outlet and validated the analytical profiles against experimental data and numerical results. Using the same mathematical model, the authors of Ref. [17] evaluate the sensitivity of the draft tube losses to the velocity field entering a Francis turbine draft tube, while the turbine is operating within a range of discharge values.

Thus, inspired by [10] and [13], it was assumed that through an automatic optimization process, an inlet velocity parameterization managed by a Genetic Algorithm could build the best velocity flow field for a particular draft tube. This will give us the opportunity to study different draft-tube flow structures provoked by different inlet velocity profiles achieving a better understanding of the flow losses.

However, the assembly of the optimization process represented a new challenge [18-19], since it was necessary to reduce the computational time of each simulation, to parameterize the inlet velocity profiles and to select the objective function to evaluate the draft tube performance.

Then, this work presents as result of an automatic optimization process, a qualitative and quantitative analysis of the draft tube flow field provoked by redesigned inlet velocity profiles. In order to suppose the perfect coupling at the runner-draft tube interface without compromising the overall flow stability of the machine, a direct correlation between the runner blade design and the kinematics of the swirl at the draft tube inlet has been established. Finally, this analysis has helped to understand how undesirable draft tube flow characteristics such as secondary flow, irregular evolution, stall and excessive velocity evolve through this important component of the turbine.

2. Optimization Process

The approach proposed to resolve this numerical optimization can be described in the following steps:

1. Inlet flow velocity profile parameterization,
2. Numerical model evaluation,
3. Optimization algorithm set-up,
4. Objective function evaluation.

The optimization strategy is built using the iSIGHT software [20], where simulation codes of different disciplines can be coupled. Optimization processes can be configured through a graphical interface with which one can set up, monitor and analyze a design problem. The optimization loop used in this work is shown in Fig 1 and the simulations codes are run via shell scripts.

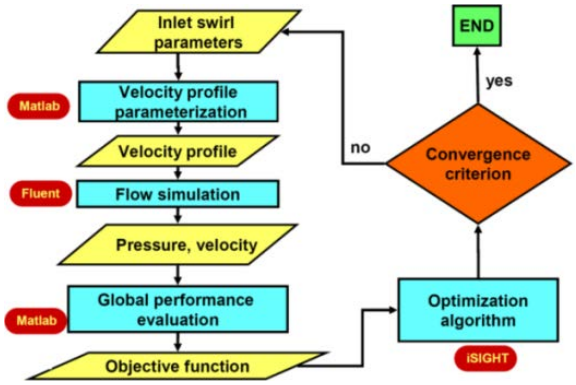

Fig 1 Flow chart of the draft tube flow optimization process.

2.1 Inlet velocity profile

The vortex equations proposed by [13] were established to represent a swirling flow produced by a constant pitch Francis runner, eq. (1-2). For the current application a Kaplan runner is used instead of a Francis therefore, modifications were applied for a better matching of the velocity equations. Specifically, a near-wall velocity profile and a near-cone hub velocity profile have

been added at each curve extremity. To handle the problem of the unknown inlet radial velocity component, a relationship between axial and radial component was used, based on a "geometrical" distribution, eq. (3). In [18-19] the high influence of the radial component on pressure distribution and pressure recovery was demonstrated computationally, in spite of the small magnitude of this velocity component.

$$V_a(r) = U_0 + U_1 e^{\left(\frac{-r}{R_1^2}\right)} + U_2 e^{\left(\frac{-r}{R_2^2}\right)} \quad (1)$$

$$V_t(r) = \Omega_0 r + \Omega_1 \left(\frac{R_1^2}{r}\right)\left[1 - e^{\left(\frac{-r^2}{R_1^2}\right)}\right] + \Omega_2 \left(\frac{R_2^2}{r}\right)\left[1 - e^{\left(\frac{-r^2}{R_2^2}\right)}\right] \quad (2)$$

$$V_r(r) = V_a \tan\theta \quad (3)$$

Thus, eight parameters were determined by fitting the experimental data and the three velocity components were imposed at section *CsIa*, as it is shown graphically in Fig 2.

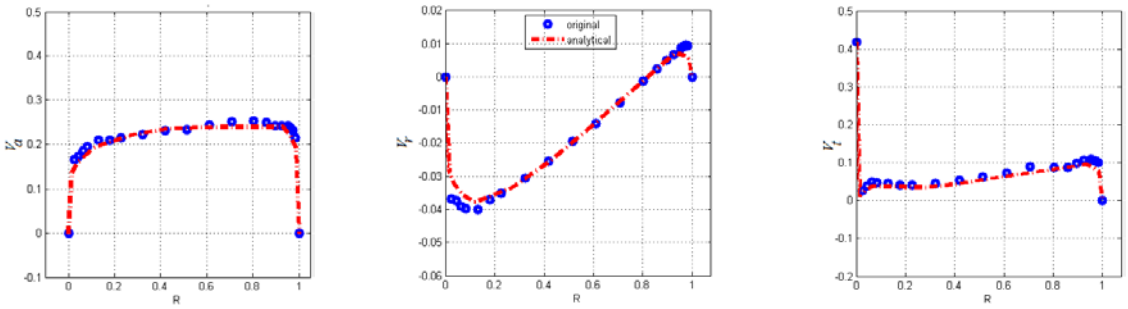

(a) Axial (b) Radial (c) Tangential

Fig 2 Original inlet velocity profiles at Best Efficient Point.

2.2 Draft tube numerical model

The *Hölleforsen* Kaplan model draft tube, located in *Indalsälven* Sweden, was used to carry out this study. This geometry, see Fig 3, has previously been used in three ERCOFTAC workshops [21-23].

These works present detailed velocity and pressure measurements at a number of sections illustrated in Fig 3(a). These measurements are used both to set the correct boundary conditions and to validate the computational results. The model used to obtain reliable numerical data during the optimization process was given by the Navier–Stokes equations. The grid, discretization and turbulence combined choices were discussed through the accuracy of k–ε turbulence models for the swirling flow in the Turbine 99 draft tube [24]. Discussion was based on graphical results and by comparing numerical simulations and experiments in the *operational mode T* (Best Efficiency Point).

A perspective view of the draft tube is shown in Fig 3(b) which presents a vertical symmetrical plane and six cross section planes where the results obtained in this work will be presented.

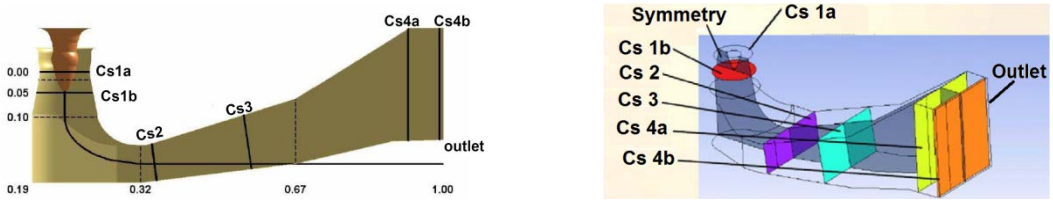

(a) Measurement points (b) 3D view sections

Fig 3 View of the study sections of the draft tube model.

2.3 Optimization Algorithm

In the present work, the optimization approach is based on an efficient Genetic Algorithm (GA) technique called Distributed GA (DGA). This method has been chosen because it is effective to seek an optimum solution in a wide design space. However, optimizations based on GA need a large number of evaluations making them better suited for a parallel computing system. This exploratory technique is established within the iSIGHT software as the Multi-Island Genetic Algorithm (MIGA). The major feature distinguishing a MIGA approach from a traditional GA is the fact that each population of individuals is divided into sub-populations called islands. The usual genetic operations (selection, reproduction and mutation) are performed separately on each island. A further operation called migration is used to transfer some individuals from an island to another. The migration process is controlled by two major parameters which are the rate of migration and the interval of migration. A parametric study was made by [25] to start an optimization loop with a high chance of success avoiding extensive preliminary sensitivity analysis proving also to

be well suited for solving highly nonlinear problems, like the present one.

2.4 Objective function

Global performance quantities including the loss coefficient factor ζ presented in eq. (4), wall pressure recovery factor Cp_w in eq. (5) and the mean pressure recovery factor Cp_m in eq. (6) were tested to select the most appropriate objective function [25]. This study revealed that ζ is highly sensitive to the changes of each inlet velocity profile parameters of each equation given by [13].

$$\varsigma = \frac{\frac{1}{A_{in}}\int_{in} P_t dA - \frac{1}{A_{out}}\int_{out} P_t dA}{\frac{1}{2}\rho\left(\frac{Q}{A_{in}}\right)^2} \tag{4}$$

Where $Pt = P+0.5\,\rho\,(u^2+v^2+w^2)$. The total loss in the flux, normalized with an energy flux estimator given by the denominator, is independent of the swirl component at the inlet.

The wall pressure recovery coefficient Cp_w given by eq. (5), is based on wall pressure considered at different points on the wall where $P_{out:wall}$ is the averaged static wall pressure across the outlet section and $P_{in:wall}$ is the averaged static wall pressure across the inlet section.

$$Cp_w = \frac{P_{out:wall} - P_{in:wall}}{\frac{1}{2}\rho\left(\frac{Q}{A_{in}}\right)^2} \tag{5}$$

In eq. (6), the mean pressure recovery Cp_m, is based on the mean values of the static pressure over the inlet and outlet areas.

$$Cp_m = \frac{\frac{1}{A_{out}}\int_{out} PdA - \frac{1}{A_{in}}\int_{in} PdA}{\frac{1}{2}\rho\left(\frac{Q}{A_{in}}\right)^2} \tag{6}$$

The loss coefficient factor ζ has also the benefit of having no restriction on the inlet flow. Thus the optimization algorithm should find the best results in a wide range of normalized inlet flows, which are defined by means of eq. (7).

$$Q_{nor} = \frac{Q}{Q_{ref}} \tag{7}$$

And the reference quantity for monitoring the numerical solution is given by the difference of mass, eq. (8).

$$imb = \dot{m}_{inlet} - \dot{m}_{outlet} \tag{8}$$

S, eq. (9), corresponds to the swirl number defined as the axial flux of swirl momentum divided by the axial flux of axial momentum.

$$S = \frac{\int_0^R (\rho V_a)(rV_t) r dr}{R\int_0^R (\rho V_a)(rV_a) dr} \tag{9}$$

Other engineering quantities of interest are the kinetic energy correction factors, one related to the axial velocity α_{ax}, in eq. (10).

$$\alpha_{ax} = \frac{1}{A_{in}u^3}\int_A u^3 dA \tag{10}$$

And the other to the swirl velocity α_{tg}, in eq. (11).

$$\alpha_{tg} = \frac{1}{A_{in}u^3}\int_A w^3 u dA \tag{11}$$

Physically α represents the ratio of the actual kinetic-energy flux, at a given cross section of an internal flow stream, to the minimum kinetic-energy flux which could exist at the particular flow rate.

The momentum correction factor, eq. (12), also called momentum coefficient or Boussinesq coefficient is the momentum of water passing through the diffuser. It is defined as the ratio of momentum of the flow per second based on actual velocity to the momentum of the flow per second based on average velocity across the section. It is denoted by:

$$\beta = \frac{1}{A_{in}u^2}\int_A u^2 dA \tag{12}$$

3. Optimization process results.

The objective function behavior with respect to each evaluation, the swirl intensity S and the flow rate Q_{nor} are presented in Fig 4. The objective function is plotted for the best individual of each generation versus the index of iteration, Fig 4(a). This graph indicates that the convergence has been reached with ζ = 0.29 % after 10×3×100 = 3000 runs. Figure 4(b) shows the variation of the objective function with respect to the inlet swirling flow intensity along the optimization process. The swirl intensity was reduced 96 % of its original value when the objective function was minimized (see Fig 4(b)). Figure 4(c) presents the variation of the mass flow rate when the objective function is minimized. Since there is no restriction to inlet mass flow, it is observed that the optimization algorithm executed the entire global search at overflow. On this account, the mass flow achieves the value of Q_{nor} = 1.86 which means that the optimized flow rate point should be out of the Best Efficiency Point of the turbine (BEP). Since there is only a single swirl number for which the objective function is minimized, the same combination axial-tangential components will maintain the energy loss factor slightly affected by the flow rate which it makes possible to scale the flow (see Table 1).

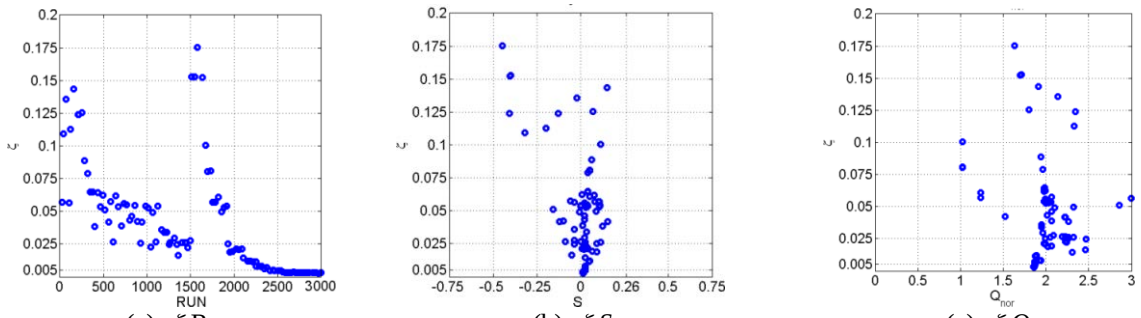

(a) ζ-Run (b) ζ-S (c) ζ-Q_{nor}

Fig 4 Objective function history presented at each generation during the optimization process.

Figure 5 shows the stochastic aspect of the MIGA to manipulate the inlet velocity parameters through the optimization process. In order to minimize the hydraulic loses the MIGA selected the vortex radius (R), the axial velocity (U) and the tangential velocity (Ω) for the three vortex equation (1-3). The initial value of zero was established for each variable of the vortex equations and its research space was 1 for the vortex radius an [-1, 1] for the axial and tangential components.

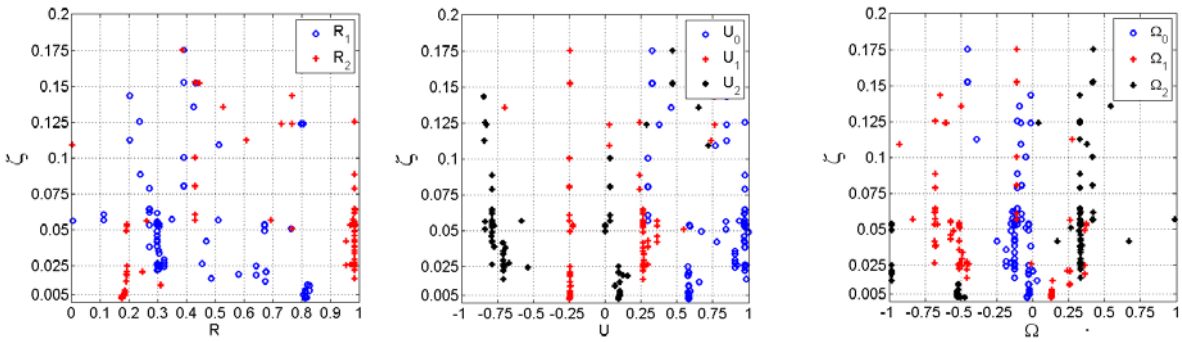

(a) ζ-Radius (b) ζ-Axial (c) ζ-Tangential

Fig 5 History of the inlet velocity profile parameters presented at each generation during the optimization process.

4. Draft tube flow analysis.

Figure 6 presents three different inlet velocity profiles obtained from the runs 256, 643 and 2,966 of the optimization process which were selected as boundary conditions to develop the quantitative and qualitative flow analysis. These velocity profiles were selected because they provoke an important step or gradient decrease of the objective function ζ, one order of magnitude, as is

shown in Table 1. The principal characteristic of these profiles with respect to the original is the near wall peak of the axial and radial components and the change of direction in the radial distribution of the tangential velocity.

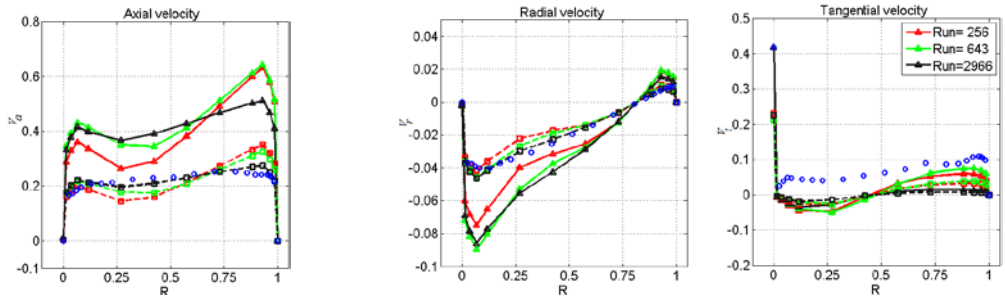

(a) Axial (b) Radial (c) Tangential

Fig 6 Inlet velocity profiles selected for the draft tube flow analysis.

All these profiles were obtained at different mass flow rates as it is shown in Table 1. However, in order to match the mass flow rate at the BEP, the inlet velocity profiles were scaled, maintaining the same swirl number. The value of the draft tube performance quantities ζ, Cp_m and Cp_w for both flow rates is very similar and the flow mass imbalance of the scaled profiles indicates a good solution of the CFD simulation. Figure 6 also presents these new scaled profiles which maintain the same relation of the axial-tangential velocity components.

Table 1 Engineering quantities reached by the selected inlet velocity profiles

RUN	Q_{nor}	Cp_m	Cp_w	ζ	S	imb
Original	1.000	0.885	1.25	0.1755	0.2600	2.58×10^{-06}
256	1.8031	0.9107	1.5814	0.1291	0.0694	1.45×10^{-04}
	1.000	0.9154	1.6866	0.1217	0.0694	3.22×10^{-04}
643	1.9738	0.9438	1.5053	0.0663	0.0759	4.50×10^{-05}
	1.000	0.9338	1.6039	0.0674	0.0759	9.00×10^{-06}
2966	1.8613	0.9352	1.3611	0.0038	0.0129	3.00×10^{-06}
	1.000	0.9264	1.4434	0.0042	0.0129	2.01×10^{-05}

4.1 Quantitative analysis

Figure 7 presents the comparisons of the draft tube performance quantities along the draft tube sections provoked by the inlet velocity profiles selected in Table 1. In Fig 7(a), the optimized profile, 2966, reduces significantly the energy loss at the inlet section *CsIa*, this is around 78% of the one generated by the original velocity profile. In order to avoid the low pressure zone just below the hub, *Cs1b*, the inlet velocity profile configuration makes the energy loss factor increase its value. However, after this zone, the flow development maintains an energy loss decrement achieving a zero value before the draft tube outlet section. The mean pressure recovery factor, Fig 7(b), and the wall pressure recovery factor, Fig 7(c), do not present the same performance order generated by the optimized flow, because the optimization was based on the energy loss factor, but even with the Cp_m, which has shown a poor sensitivity, the efficiency increment is significant, reaching 4.14%.

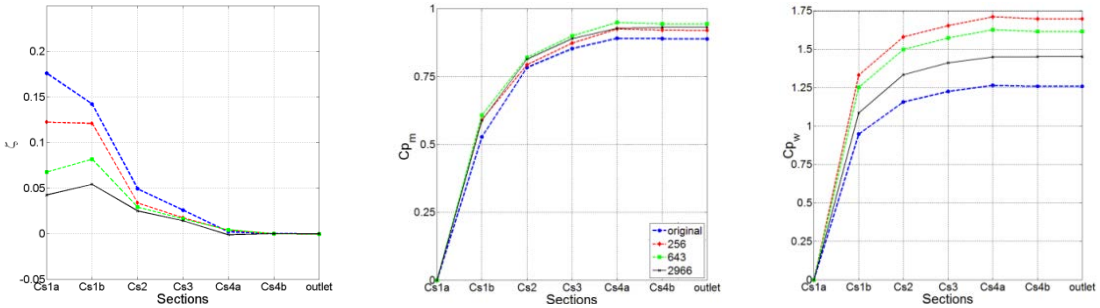

(a) ζ (b) Cp_m (c) Cp_w

Fig 7 Energy loss factor and pressure recovery developed along the draft tube.

Figure 8 presents the draft tube performance evaluated along the draft tube by considering eq. (9-12). Figure 8(a) shows the effect of the non-uniformity in the velocity profile by the axial kinetic energy factor α_{ax}. Since diffusion requires a reduction in kinetic energy flux, any increase in the non-uniformity represents an increase of α_{ax}. The optimized profiles reduce this factor at the downstream section *Cs4a*. The amount of kinetic energy of the tangential velocity component is quantified in Fig 8(b) and represents the augmentation of actual kinetic energy due to swirl. The optimized profiles achieve a reduced number along all the draft tube length due to sufficient diffusion provoked by a lower swirl number. Figure 8(c) presents the momentum correction factor which is the momentum of water passing through the diffuser and it is different from the unity when the velocity across a flow area is not uniform. The optimized flow shows a better approximation to this value at the end of the draft tube. Figure 8(d)

presents the swirl intensity along the diffuser. For the optimized flow, this quantity is maintained almost constant throughout the draft tube except at the end, where it undergoes a slight increase. On the contrary, the other flows suffer a drop of the swirl intensity at the end that provokes a wall flow detachment.

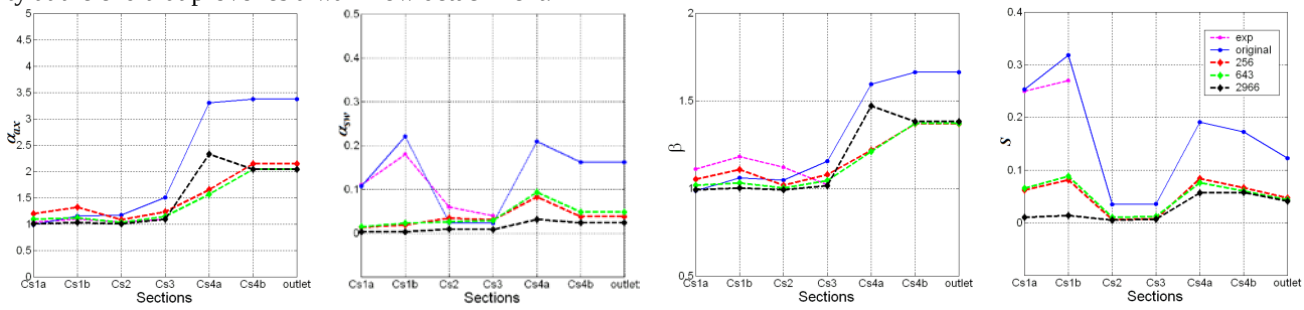

(a) α_{ax} (b) α_{tg} (c) β (d) S

Fig 8 Engineering quantities along draft tube sections.

4.2 Qualitative analysis

Figure 9 presents the total pressure contours provoked by the original flow and the optimized ones, at the draft tube symmetry plane. Stronger decrease of the total pressure zone is obtained by the optimized profiles at the *CsIb* section, Fig 8(d). The pressure reduction below the runner hub zone indicates back-flow mean velocity. The radial and axial velocity gradients near the wall raise the pressure on the wall, avoiding flow separation and consequently low pressure regions beneath the runner hub, which decreases considerably in the optimized flow. This allows a homogeneous pressure distribution downstream, because there is no adverse pressure gradient in the elbow zone. As such, the flow generated by the optimized profiles affect the draft tube function through a blockage effect.

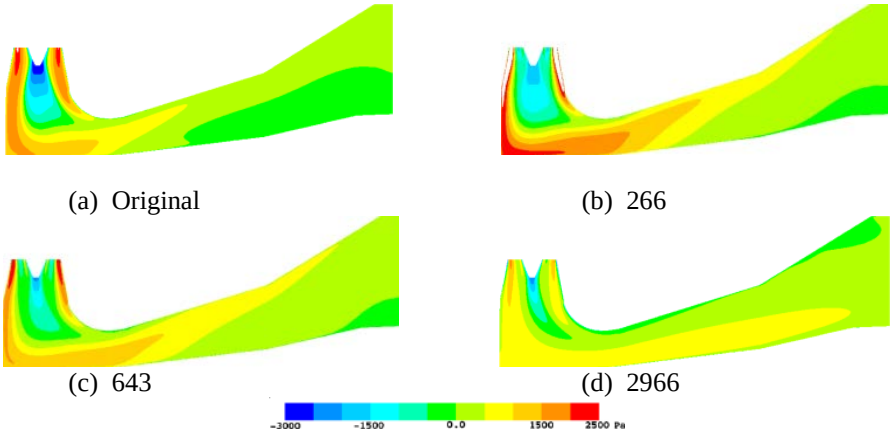

(a) Original (b) 266

(c) 643 (d) 2966

Fig 9 Total pressure contours at the draft tube symmetry.

The streamlines and vectors at several cross sections are shown in Fig 10 for the original and optimized inlet flows. The picture reveals asymmetric structures in the secondary flow, due to the change of rotational direction at the inlet. While the tangential velocity component exists in all the original sections, in the optimized sections this component is reduced up to practically disappearing except for a strong radial component towards the cone wall. The streamlines in the sections *Cs2* and *Cs3* indicate two counter-rotating vortices on each side of the centerline. The left vortex seems to be stronger than that of the right side. For the optimized flow, the counter-rotating vortices have a lower intensity and they are finally displaced to the lower wall. Almost the same flow pattern continues downstream along the next sections *Cs4a*, *Cs4b* and the outlet. At the outlet section, both the original and optimized flow maintains the secondary flow with a high intensity vortex zone in the upper left corner.

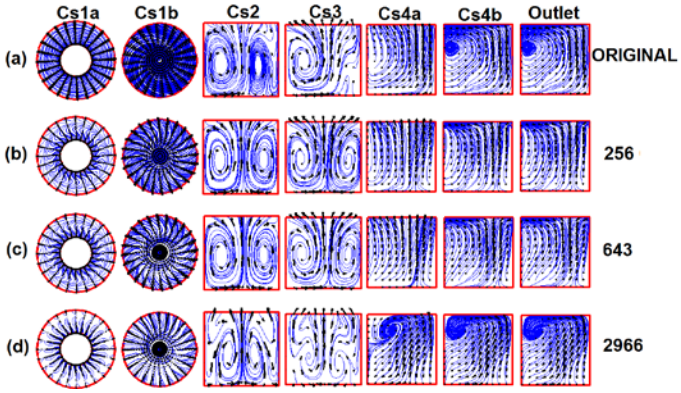

Fig 10 Streamlines and vectors at draft tube sections provoked by the inlet velocity profiles. (flow coming towards the reader)

Figure 11 presents the axial velocity contours at different draft tube cross sections. At the inlet section *Cs1a*, the principal difference among axial velocity profiles lies in the radial distribution of its magnitude. At section *Cs1b*, the axial velocity magnitude has been reduced, however, in the original profile, there is a large area of back flow downstream of the rotating hub. Inversely, for the optimized profiles this area is progressively reduced. At the downstream sections, the picture reveals a reduction of the main flow towards the left side, in the original flow, with back-flow at the lower wall. In the optimized flow, Fig 11(d), the zone with no main flow agrees with the vortex zone presented in Fig 11(d), whereby it is argued that back flow is not present at the outlet section of the optimized flow.

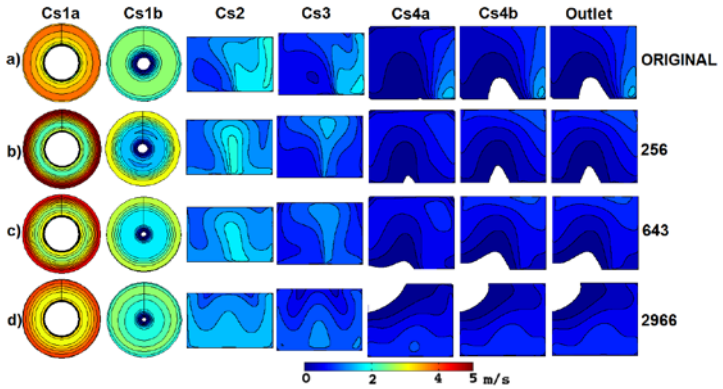

Fig 11 Axial velocity contours at the draft tube sections provoked by the inlet velocity profiles.
(flow coming towards the reader)

Figure 12 shows the streamlines and vectors at the symmetry mid-plane from draft tube inlet to outlet. Due to the changes of rotation direction along the inlet radius and the near-wall axial velocity increase for the optimized profile, as is presented in Fig 6, the main flow moves to the lower wall and consequent bend blockage and back-flow beneath the hub are suppressed. In these figures it can be appreciated that the main velocity uniformity is increased by the optimized flows, and the back-flow at the outlet section has been suppressed.

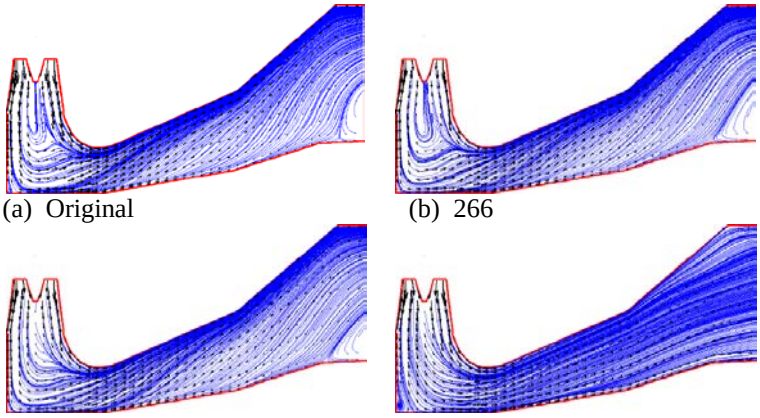

(a) Original (b) 266

(c) 643 (d) 2966

Fig 12 Streamlines and vectors at the draft tube symmetry provoked by inlet velocity profiles.
(flow coming towards the reader)

Figure 13 shows the total pressure contours along the draft tube sections. It is clear that in the first two sections the radial pressure distribution is more uniform as the inlet velocity profile is optimized. The negative pressure core in section *Cs1b* is reduced dramatically in the run 2966 in relation to the original profile. This seems to provoke an important gain in the total pressure at the end of the cone which could explain the higher value of the energy loss factor in this section, Fig 7(a). In the next draft tube sections the total pressure presents a better distribution because its contours are symmetrical and uniform when the inlet velocity profile is optimized.

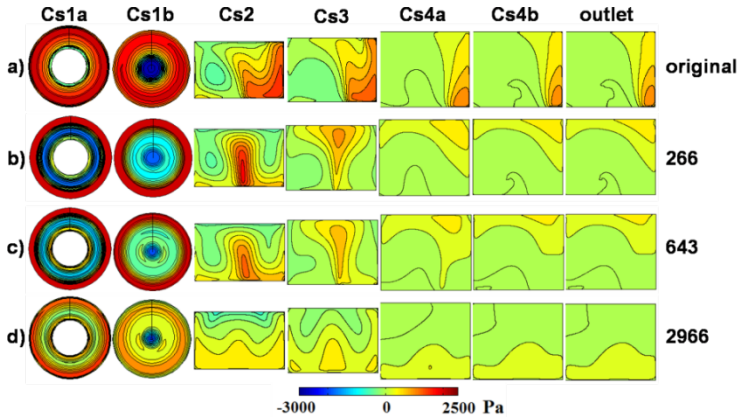

Fig 13 Total pressure contours at the draft tube sections provoked by the inlet velocity profiles.

4.3 Flow angle

The direct correlation between the runner blade design and the kinematics of the swirl on the draft tube inlet is established by the relative flow angle eq. (13) and given by [13].

$$Flow\,angle = \arctan\frac{V_a}{r - V_t} \tag{13}$$

The velocities were rendered dimensionless using the rotational speed, and the radius using the inlet radius as a reference. This is why the flow angle relates the dimensionless axial velocity (V_a) to the dimensionless relative circumferential velocity (r-V_t). So, the flow angle only depends on the exit angle of the blades, provided that the flow remains attached. This is the case for a turbine runner operating near the best efficiency point (BEP).

An important property of the swirling flow downstream a constant pitch hydraulic turbine runner is that the relative flow angle depends only on the blade exit angle provided that the flow remains attached. The significant changes in the circumferential and axial velocity profiles in the survey section can be associated to the upstream variation of the blade trailing edge as it is shown in Fig 14. The flow angle seems to fit the experimental data and the blade trailing edge will not suffer an important modification with regard to the original blade angle. This parameter could be used as a quantitative correlation between the swirling flows sought at the draft tube inlet and blade shapes that can be easily produced.

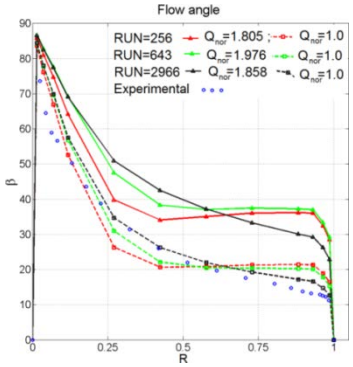

Fig 14 Flow angle computed in the survey section for the different vortex structures

5. Conclusion

In order to improve the runner-draft tube coupling, an optimization process of the velocity profiles at the draft tube inlet was developed using numerical tools. This process allowed determining the profile for which the minimum energy loss factor was reached. Three theoretical inlet velocity profiles generated by a Kaplan runner were selected to study the qualitative and quantitative flow structure along the draft tube. The results obtained clearly illustrate the importance of the flow uniformity after the elbow at the end of the conduit. If the momentum parameter can be reduced in the last draft tube sections, the draft-tube performance is increased considerably. At the end of the hub, the optimized profile must increase its energy loss factor in order to reduce the negative total pressure. Another important aspect is the elimination of the re-circulating flow at the elbow zone caused by a blockage which promoted an adverse pressure gradient in the cone, deteriorating the pressure recovery effect. Also, the flow angle could be used as a quantitative correlation between the swirling flow sought at the draft tube inlet and blade shapes. This could filter non realistic runner blades during a distinct optimization process. Finally, it can be stated that the results of this optimization methodology helped us understand how the inlet flow characteristics can be changed in order to suppress undesirable effects such as secondary and back flow, irregular evolution and excessive swirling intensity along a specific draft tube.

Nomenclature

V_a	Dimensionless axial component of velocity [-]	R	Outer radius of the cone
V_t	Dimensionless tangential component of velocity [-]	θ	Cone half opening angle
V_r	Dimensionless radial component of velocity [-]	Cpw	Wall pressure recovery factor
R_s	Dimensionless radius of the survey section [-]	Cpm	Averaged pressure recovery factor
R	Dimensionless vortex core radii	A_{in}, A_{out}	Inlet and outlet areas
Ω	Dimensionless angular velocities	Q	Flow rate
U	Dimensionless axial velocities	P_t	Total pressure
R	Dimensionless radius	Q_{ref}	Reference flow rate
u, v, w	Cartesian velocity components of V		
$r\text{-}V_t$	Dimensionless relative circumferential velocity		

References

[1] Falvey, H., 1993, "A primer on draft tube surging", Hydro Review (February), 12(1) pp. 77-86.

[2] Tridon, S., Barre, S., Ciocan, G-D, and Tomas, L., 2010, "Experimental analysis of the swirling flow in a Francis turbine draft tube: Focus on radial velocity component determination". European Journal of Mechanics B/Fluids 29(4) pp.321-335.

[3] Nishi, M., and Liu, S., 2013, "An outlook on the Draft-Tube-Surge Study" International Journal of Fluid Machinery and Systems, 6(1), 33-48.

[4] Falvey, H., and Cassidy, J., 1970, "Frequency and amplitude of pressure surges generated by swirling flows" In Proceedings of the International Association for Hydraulic Research. Symposium on Hydraulic Machinery and Cavitation. Stockholm Sweden, No. **E1** 1–12.

[5] Padle, U., 1974, "Model and prototype turbine draft tube surge analysis by the swirl momentum method", In Proceedings of the International Association for Hydraulic Research. Symposium on Hydraulic Machinery and Cavitation. Stockholm Sweden No. III 1–13.

[6] Monacelli, G., and Cooper, P., 1987, "Performance of draft tubes for small-hydropower turbine", In Water Power'87 1200-1209 ASCE.

[7] Kubota, T., Han, F., and Avellan, F., 1996, "Performance analysis of draft tube for GAMM Francis turbine", In Proceedings of the XVIII IAHR Symposium, Hydraulic Machinery and Cavitation. Dordrecht NL No. 1 pp. 130-139.

[8] Shyy, W., and Braaten, M., 1986, "Three-dimensional analysis of the flow in a curved hydraulic turbine draft tube", International Journal of Numerical Methods in Fluids 6(12) pp.861-882..

[9] Vu, T., and Shyy, W., 1990, "Navier-Stokes flow analysis for hydraulic turbine draft tubes", Journal of Fluids Engineering 112(2) pp. 119-204.

[10] Vu, T., 1989, "A design parameter study of turbine draft tube by viscous flow analysis", WATERPOWER'89 pp. 557-566.

[11] Mauri, S., Kueny, J., and Avellan, F., 2002, "Werlé-Legendre separation in a hydraulic machine draft tube", In ASME 2002 Fluids Engineering Division Summer Meeting, Montreal, Québec Canada.

[12] Vu, T. C., Devals, C., Zhang, Y., Nennemann, B., & Guibault, F. (2011, March). "Steady and unsteady flow computation in an elbow draft tube with experimental validation". International Journal of Fluid Machinery and Systems, 4(1), pp. 85-96.

[13] Susan-Resiga, R., Ciocan, G., Anton, I., and Avellan, F., 2006, "Analysis of the Swirling Flow Downstream a Francis Turbine Runner", ASME J. Fluids Eng., 128(1), pp. 177–189.

[14] Gagnon, J., Iliescu, M., Ciocan, G., and Deschênes, C., 2008, "Experimental Investigation of Runner Outlet Flow in Axial Turbine With LDV and Stereo- scopic PIV", 24th IAHR Symposium on Hydraulic Machinery and Systems, Foz do Iguassu, Brazil, October, pp. 27–31.

[15] Gagnon, J.-M., Aeschlimann, V., Houde, S., Flemming, F., Coulson, S., and Deschênes, C., 2012, "Experimental Investigation of Draft Tube Inlet Velocity Field of a Propeller Turbine", ASME J. Fluids Eng., 134(10), p. 101102.

[16] Muntean, S., Ciocan, T., Susan-Resiga, R., Cervantes, M., and Nilsson, H., 2012, "Mathematical, Numerical and Experimental Analysis of the Swirling Flow at a Kaplan Runner Outlet", Earth and Environmental Science (IOP Conference Series), Vol. 15, IOP Publishing, p. 032001.

[17] Susan-Resiga, R., Muntean, S., Ciocan, T., Joubarne, E., Leroy, P., and Bornard, L., 2012, "Influence of the Velocity Field at the Inlet of a Francis Turbine Draft Tube on Performance Over an Operating Range", Earth and Environmental Science (IOP Conference Series), Vol. 15, IOP Publishing, p. 032008.

[18] Galván, S., Reggio, M., and Guibault, F., 2012, "Optimization of the inlet velocity profile in a conical diffuser", ASME 2012 Fluids Engineering Summer Meeting, Rio Grande, Puerto Rico, USA, FEDSM2012-72103.

[19] Galván, S., Reggio, M., and Guibault, F., 2013, "Inlet velocity profile optimization of the turbine 99 draft tube", ASME 2013 Fluids Engineering Summer Meeting, Incline Village Nevada USA, FEDSM2013-16473.

[20] isight, 1994, iSIGHT 9.0.1 *Engineous Software Inc*.

[21] Gebart, B., Gustavsson, L., and Karlsson, R, 2000, "Proc. of Turbine-99 – Workshop on draft tube flow", Luleå University of Technology, Technical Report 2000:11.

[22] Engström, T., Gustavsson, L., and Karlsson, R., 2001, "Proc. of Turbine-99 –Workshop 2", Luleå University of Technology.

[23] Cervantes, M., Engström, T., and Gustavsson, L, 2005, "*Proc. of Turbine-99 III"*, Luleå University of Technology, Technical Report 2005:20.

[24] Galván, S., Reggio, M., and Guibault, F., 2011, “Assessment study of k−ε turbulence models and near-wall modeling for steady state swirling flow analysis in draft tube using Fluent”, Eng. Appl. Comput. Fluid Mech., 5(4) pp. 459-478.
[25] Galván S., Rubio, C., Pacheco, J., Mendoza, C., and Toledo, M., 2013, “Optimization Methodology Assessment for the Inlet Velocity Profile of a Hydraulic Turbine Draft Tube Part I: Computer Optimization Techniques”, Journal of Global Optimization 55(1) pp. 53–72.